THE JOURNAL OF BIOLOGICAL CHEMISTRY
Vol. 276, No. 20, Issue of May 18, pp. 17307–17315, 2001

Printed in U.S.A.

Activation of Cell Division Protein FtsZ

CONTROL OF SWITCH LOOP T3 CONFORMATION BY THE NUCLEOTIDE γ-PHOSPHATE*

Received for publication, December 4, 2000
Published, JBC Papers in Press, January 25, 2001, DOI 10.1074/jbc.M010920200

José Fernando Díaz‡§, Andrew Kralicek‡, Jesús Mingorance¶, Juan Manuel Palacios‡, Miguel Vicente¶, and José Manuel Andreu‡

From the ‡Centro de Investigaciones Biológicas, Consejo Superior de Investigaciones Científicas, C/Velázquez, 144, 28006 Madrid and the ¶Centro Nacional de Biotecnología, Consejo Superior de Investigaciones Científicas-Campus de Cantoblanco, 28049 Madrid, Spain

The effect of bound nucleotide on the conformation of cell division protein FtsZ from *Methanococcus jannaschii* has been investigated using molecular dynamics and site-directed mutagenesis. The molecular dynamics indicate that the γ-phosphate of GTP induces a conformational perturbation in loop T3 (Gly^{88}-Gly^{99} segment), in a position structurally equivalent to switch II of Ha-*ras*-p21. In the simulated GTP-bound state, loop T3 is pulled by the γ-phosphate into a more compact conformation than with GDP, related to that observed in the homologous proteins α- and β-tubulin. The existence of a nucleotide-induced structural change in loop T3 has been confirmed by mutating Thr^{92} into Trp (T92W-W319Y FtsZ). This tryptophan (12 Å away from γ-phosphate) shows large differences in fluorescence emission, depending on which nucleotide is bound to FtsZ monomers. Loop T3 is located at a side of the contact interface between two FtsZ monomers in the current model of FtsZ filament. Such a structural change may bend the GDP filament upon hydrolysis by pushing against helix H8 of next monomer, thus, generating force on the membrane during cell division. A related curvature mechanism may operate in tubulin activation.

FtsZ and tubulin are proteins essential for cell division. Tubulin αβ-dimers self-assemble into eukaryotic microtubules (1), whereas FtsZ is a main component of the prokaryotic septation ring (2). The functions of these proteins make them obvious targets for antitumor drugs (tubulin) or for a possible new generation of antibiotics (FtsZ).

FtsZ together with tubulin form a distinct group of GTPases (3–6), which form in turn structural polymers. Tubulin assembles into microtubules, hollow cylinders composed of longitudinal protofilaments (7), whereas FtsZ polymerizes *in vitro* into microtubule-related filaments (8, 9). A third GTPase, dynamin (10), whose possible structural relationship with FtsZ and tubulin is presently unknown, shares with FtsZ organelle division functions (11, 12) and is able to *in vitro* self-assemble into ring-shaped oligomers and helical polymers (13).

The structures of FtsZ and tubulin have a common fold and are remarkably similar (14, 15). FtsZ and tubulin have a limited structural similarity with the small G-proteins of the *ras* type (16). FtsZ, tubulin, and the *ras* proteins also share the function of molecular switches activated by GTP. The activated protein is able to interact with a target protein (downstream signal transmission), the interaction being heterophilic in the cases of *ras*, and homophilic in the case of the structural GTPases.

The lifetime of the activated state of these proteins is regulated by the interaction with GTPase-activating proteins (GAPs)[1] (17), which provide an external residue to the active center that stabilizes the existing catalytic machinery (18) (upstream signal transmission). As in the case of the downstream signal transmission, in *ras* this upstream interaction is heterophilic, since the GAP, *ras*, and the target are different proteins. In the case of the structural GTPases FtsZ and tubulin, the upstream interaction is also homophilic, since the GAP is as well FtsZ or tubulin (16). So the GAP-activated protein, activated protein-target interactions are identical, with the net result being the formation of a homopolymer. That means the activation/deactivation process of the structural GTPases is conceptually identical but biochemically much simpler than in the case of *ras*-like proteins. The protein to which the signal is transmitted and the one that provides the additional residue that activates the GTPase are identical, *i.e.* another molecule of tubulin or FtsZ. Thus, the structural GTPases constitute an ideal system for studying molecular signal transmission as identical protein molecules transmit, receive, and interrupt the signal transmission.

Information about the nature of the structural changes that the binding of an activator induces in a protein molecule, and how the activation signal is transmitted, can be obtained by comparing the structures of the initial and final stages of the activation transition. Nevertheless, little can be deduced about the mechanism of molecular activation from the presently available x-ray crystal structure of GDP-bound FtsZ from *Methanococcus jannaschii* (14) and the 3.7-Å resolution electron crystallographic structure of αβ-tubulin in zinc-induced polymers (15).

A useful approach to study conformational transitions in proteins is the use of computational methods. Knowing the structure of GDP-bound FtsZ, it is possible to introduce a γ-phosphate into the molecule and study the perturbations induced in the protein structure. The computational methods

* This work was supported in part by Comisión Interministerial de Ciencia y Tecnología (Spain) Grants BIO99-0859-C03-02-03 and BIO97-1246 and by Programa de Grupos Estratégicos de la Comunidad Autónoma de Madrid. The costs of publication of this article were defrayed in part by the payment of page charges. This article must therefore be hereby marked "*advertisement*" in accordance with 18 U.S.C. Section 1734 solely to indicate this fact.

§ Recipient of a contract from Programa de Incorporación de Doctores a Grupos de Investigación en España. To whom correspondence should be addressed. Tel.: 34-915611800 (ext. 4380); Fax: 34-915627518; E-mail: fer@akilonia.cib.csic.es.

¶ Recipient of a fellowship from Programa de Estancia de Científicos y Tecnólogos Extranjeros en España.

[1] The abbreviations used are: GAP, GTPase-activating protein; PCR, polymerase chain reaction; HPLC, high performance liquid chromatography; WT, wild type; r.m.s., root mean square.

employed are based on molecular dynamics (19–21), in which simulations of the solution structures with GDP and GTP bound on the nucleotide site are compared. In principle, a long enough molecular dynamics simulation should be able to find the structures of the inactive GDP-bound form (which may diverge from the starting crystal structure), and of the active GTP-bound form of FtsZ. Unfortunately, the calculations may tend to stay in local minima and the equilibration time needed might be much longer than the maximum simulation time presently affordable (nanosecond). Nevertheless, it is still possible to obtain useful information about the system by studying the perturbations induced in the structure by the presence of the γ-phosphate. These procedures were successfully employed, in combination with targeted molecular dynamic techniques (19), to predict the hinges of the conformational transition between the active and the inactive state of Ha-*ras*-p21 (20, 21). These predictions have been experimentally confirmed (22–24).

The *Methanococcus* genus of methanogenic archea consists of five species, all of them hyperthermophiles (25). The stability of proteins in these archea is seriously compromised by the high temperatures of their habitats, the folded state of the proteins being favored by a higher concentration of chaperones, the accumulation of certain solutes like 2,3-cyclic diphosphoglycerate and certain modifications of the sequence that produce a larger number of salt bridges and increase the hydrophobicity of the core (mutations that introduce holes in the hydrophobic core of hyperthermophile proteins seriously compromise their stability (26)). FtsZ from *M. jannaschii* should be expected to be extremely stable at the relative low temperature (300 K) at which the simulations are performed, so that any movements detected when the γ-phosphate group is introduced into the structure should be probably more related with the activation state of the protein.

In this paper the solvated GDP and GTP-bound molecular dynamics-calculated structures are compared with the crystal structure of FtsZ from *M. jannaschii* (14). Structural changes found in zones potentially functional in activation for assembly are here described. A single tryptophan mutant at loop T3 has been designed according to molecular dynamics predictions, whose fluorescence properties monitor the GDP or GTP nucleotide bound to the protein.

EXPERIMENTAL PROCEDURES

Protein Purification and Characterization—$MgCl_2$, EDTA, KCl, and Tris were from Merck. GDP was from Sigma and GTP (lithium salt) from Roche Molecular Biochemicals. Guanidine hydrochloride was from Calbiochem. Other analytical grade chemicals were from Merck or Sigma, except as otherwise indicated.

FtsZ from *M. jannaschii* (FTSZ1 or MJ0370) was expressed in *Escherichia coli* BL21/C41 as described (14). This wild type FtsZ has a single tryptophan at position 319. The T92W-W319Y mutant FtsZ was constructed using a modified version of the inverse-PCR site-directed mutagenesis protocol of Ref. 27. The first step toward producing this double mutant of FtsZ was to make the W319Y FtsZ mutant. Inverse PCR was performed using the Excite High Fidelity PCR System (Roche Molecular Biochemicals), the plasmid pHis17-mjFtsZ-H (28) as template, and the following 5′-phosphorylated primers: p319Tyr (ATATATAATTGTAGCATTTGGGTCTAATCTTG), which results in changing Trp^{319} to Tyr; and p319NarI (GGCGCCACAATAGATGAGAACTTAG), which introduces an adjacent silent restriction site marker, *Nar*I, that is unique to the plasmid. The PCR parameters were 1 cycle of 5 min at 95 °C; followed by 15 cycles of 15 s at 95 °C, 30 s at 55 °C, and 4 min at 68 °C, terminating with 1 cycle of 20 min at 68 °C. The PCR product was purified with the Concert Rapid PCR Purification System (Life Technologies, Inc.) and polished with the *Pwo* DNA polymerase (Roche Molecular Biochemicals) to remove any additional nucleotides added to the 3′ end of the PCR product by the Excite High Fidelity polymerase. The polished PCR product was purified, ligated by T4 DNA Ligase (Roche Molecular Biochemicals), and then digested with *Dpn*I enzyme (Promega) to reduce the level of parental plasmid. The ligated PCR product was then transformed into *E. coli* DH5α cells and the desired transformants selectively grown on LB plates containing 50 μg/ml ampicillin and 50 μg/ml chloramphenicol. Plasmid DNA was purified from individual transformants using the Concert Rapid Plasmid Purification system (Life Technologies, Inc.), and the mutant plasmid, pAVK1(W319Y) identified by digestion with *Nar*I, followed by the sequencing of the gene for FtsZ with sequencing primers mf3 (ACCATATCTGAATCTTG), mj1r (CGGCATATTTGGAAC), and p319Tyr. The double mutant of FtsZ was then obtained in an identical manner, except the PCR template was pAVK1(W319Y) and the primers were pHindT92W (TAAAAAGCTTTGGAGAGGTCTTGGAGC), which results in changing Thr^{92} to Trp and introduces the adjacent silent restriction marker, *Hin*dIII (of which there is one other site in the plasmid), and pantiHind (CCAATTAATATTTTTTTATCAGC). The double mutant plasmid, pAVK2 (T92W-W319Y) was identified by *Hin*dIII digestion, sequenced as before, and transformed into *E. coli* BL21:pLys for overexpression by induction with 1 mM isopropyl-1-thio-β-D-galactopyranoside.

The proteins were purified as described in Ref. 14 except that the *E. coli* cells containing the protein were lysed by five 30-s sonication cycles instead of by heat shock. For comparative purposes the wild type protein was as well purified by a heat shock (14). Both proteins were stored at −70 °C and equilibrated in the desired buffer prior to use. Protein purities were checked by SDS-polyacrylamide gel electrophoresis (29) and were found to be >98% for all three purified proteins. Protein concentrations were measured by taking their UV spectra in 6 M guanidine hydrochloride, after subtracting the contribution of nucleotide, which was measured and characterized by HPLC as described (30). The extinction coefficients employed (280 nm) were 8100 M^{-1} cm^{-1} for guanosine nucleotides,[2] and 1280 M^{-1} cm^{-1} for tyrosine and 5690 M^{-1} cm^{-1} for tryptophan (31). The total Mg^{+2} and Ca^{+2} concentrations were measured by atomic absorption spectrometry with a PerkinElmer Life Sciences model 2380 spectrometer.

The relative affinity of the proteins for GDP and GTP was checked by incubating 25 μM FtsZ (WT or T92W-W319Y) for 1 h at 4 °C in buffer A (50 mM Tris, 50 μM EDTA, 10 μM GDP, pH 8.0), 500 mM KCl plus 5, 10, 50, 100, or 200 μM GTP. The excess nucleotide was removed by a chromatography in a 5-ml Hitrap desalting fast protein liquid chromatography column equilibrated in 50 mM Tris, 50 μM EDTA, 500 mM KCl, pH 8.0, containing 10 μM [GTP + GDP], where the GDP/GTP ratio was the same as in the incubation mixture. The nucleotide content of the mixture was characterized by HPLC (30).

Laser desorption/ionization mass spectroscopy measurements were performed on a BIFLEX time-of flight instrument (Bruker-Franzen Analytik, Bremen, Germany) operated in the positive mode. Samples were analyzed in the linear mode, and typically 100 laser shots were summed into a single mass spectrum. External calibration was performed using bovine serum albumin (M_r 66,432.9) as standard. The molecular mass values obtained were 39,817 ± 80 for the wild type (theoretical 39,891.2), and 39,975 ± 80 (theoretical 39,953.2) for the T92W-W319Y double mutant.

The fluorescence emission spectra of the proteins in their GDP- and GTP-bound state were measured at 25 °C employing a Shimadzu RF-540 spectrofluorimeter (excitation wavelength, 295 nm; 5-nm excitation and emission slits)

The circular dichroism spectra of the proteins (10 μM FtsZ) equilibrated in Buffer A, 500 mM KCl, plus 50 μM GDP or GTP were measured at 25 °C employing a JASCO J720 dichrograph, using 0.1-cm cells. The contents in the secondary structure were estimated by deconvolution of the CD spectra using the convex constraint algorithm method (32).

Sedimentation equilibrium and velocity measurements were performed at 25 °C in an Optima XL-A (Beckman-Coulter) analytical Ultracentrifuge as described (33). Whole-cell apparent average molecular weights of FtsZ were obtained using the program EQASSOC (34). Sedimentation coefficients were calculated by global fitting of multiple sedimentation profiles with the program SVEDBERG (retrieved from the RASMB server (35)).

Molecular Dynamics—The starting structure of the GDP form (1FSZ) (14) of FtsZ from *M. jannaschii* was obtained from the Brookhaven Protein Data Bank (36). The starting coordinates for the simulation of the conformation of FtsZ bound to GTP were those of the GDP form with a γ-phosphate added to the GDP (the coordinates of the γ-phosphate were obtained by overimposing the GDP bound to FtsZ with the GTP bound to the α-tubulin subunit (1TUB); Ref. 15). Since no Mg^{+2} was found to be bound to the purified protein as described by Löwe and

[2] J. F. Díaz and J. M. Andreu, unpublished data.

Amos (14), and no Mg^{+2} coordinates were available in the $\alpha\beta$-tubulin heterodimer (15), the uncertainty in the position of possible Mg^{+2} cation bound to the protein was too high to model it in the nucleotide site. The GROMOS 96 software package (37) was obtained from BIOMOS b.v. (Groningen, The Netherlands). The Protein Data Bank format of the structure files was transformed into GROMOS 96 format using the *procs2* routine of the software package, then the polar hydrogen coordinates were generated using *progch*, and the resulting structure was included into a 87-Å-wide truncated octahedral water box of single point charge water (38) where a minimum distance of 8 Å was kept between the protein and the border of the box. The energy of the resulting structure was minimized for 500 steps using a steepest descent algorithm (39), and counterions (Cl^- and Na^+) were added to neutralize the charges of the system. The systems simulated with GDP and GTP bound contained 31,162 and 31,158 atoms, respectively. The system was then energy-minimized for another 500 steps. The minimized structures were found not to diverge from the Protein Data Bank structure (r.m.s. deviation 0.01 and 0.02 Å for the GDP- and GTP-bound minimized structures, respectively). The velocities of the atoms were then randomly assigned to a Maxwellian velocity distribution at 300 K and three different free molecular dynamics simulation of each system (D1, D2, and D3 for the GDP-bound structure and T1, T2, and T3 for the GTP-bound structure), with different starting Maxwellian velocity distributions assigned, were performed for 500 ps using a constant pressure of 1 atm and a constant temperature of 300 K. The temperatures of the protein and the solvent were separately coupled to a water bath (40) using a coupling constant of 0.1 ps. The pressure was kept constant by coupling to an external pressure bath (40) with a coupling constant of 0.5 ps. The conditions of the MD simulation were the following: the time step employed was 2 fs, the integration of the equations of motion was done using the leapfrog algorithm included in the GROMOS 96 package, the bond lengths were constrained to equilibrium values using the SHAKE routine (41, 42), and a cutoff of 8 Å was used for nonbonded interactions and 14 Å for electrostatic interactions. For analysis the coordinates and velocities were saved every 0.5 ps. For the calculation of the r.m.s. deviation, the structures were fitted using a least-squares fit of the Cα atoms. The calculations were performed using the parallelized version of *promd* in a Challenge 10000 Silicon Graphics workstation equipped with two MIPS R10000 processors. Each 500-ps simulation required 80 days (160 days of CPU time). The data were analyzed using SIMLYS version 3 (43).

Quality of the Molecular Dynamics Simulations: r.m.s. Deviations and Energy—Fig. 1 (*A* and *B*) shows the r.m.s. deviation of the simulated solution structures of GDP-bound and GTP-bound FtsZ from the crystal structure of the GDP-bound form of the protein. In five of the six simulations, an equilibration time of 200 ps is enough to reach plateau values (GDP: D1 1.64 ± 0.08 Å, D3 1.87 ± 0.14 Å; GTP: T1 1.75 ± 0.10 Å, T2 1.52 ± 0.06 Å, T3 1.90 ± 0.31 Å). The apparently different behavior of one GDP simulation (D2, which reaches a rapid equilibrium, like the others, after 60 ps, but between 300 and 400 ps undergoes a relatively large deviation; see Fig. 1*A*) is simply due to rotation around the Thr^{36}-Lys^{37} bond, which changes the position of the helix H0 without altering its structure (data not shown). The r.m.s. deviation of this simulation (D2), calculated without taking into account helix H0, stabilizes after 300 ps at a plateau value of 1.55 ± 0.07 Å, similarly to the other simulations.

The last 50 ps of each simulation were averaged to obtain the final average structures. The three final average structures with each nucleotide (GDP: D1s, D2s, D3s; GTP: T1s, T2s, T3s) were compared and found to be very similar except for some differences in the position of the H0 helix, and of the loop from Ile^{251} to Ala^{265} (r.m.s. deviation values: D1s-D2s 1.54 Å, D1s-D3s 1.43 Å, D2s-D3s 1.53 Å, T1s-T2s 1.61 Å, T1s-T3s 1.53 Å, T2s-T3s 1.49 Å).

Fig. 2 (*A* and *B*) show the evolution of the potential energy of the systems. The initial potential energy of both forms is equal in all simulations (−395 MJ mol^{-1}) and drops very rapidly (1 ps) to values of approximately −444 MJ mol^{-1}, then an equilibration time of 100 ps is required to reach a slightly lower plateau for the GTP simulations than for the GDP simulations (T1 −450.7 ± 0.5 MJ mol^{-1}, T2 −450.8 ± 0.5 MJ mol^{-1}, T3 -450.5 ± 0.8 MJ mol^{-1}, D1 -449.6 ± 0.6 MJ mol^{-1}, D2 -449.9 ± 0.5 MJ mol^{-1}, D3 −449.7 ± 0.5 MJ mol^{-1}).

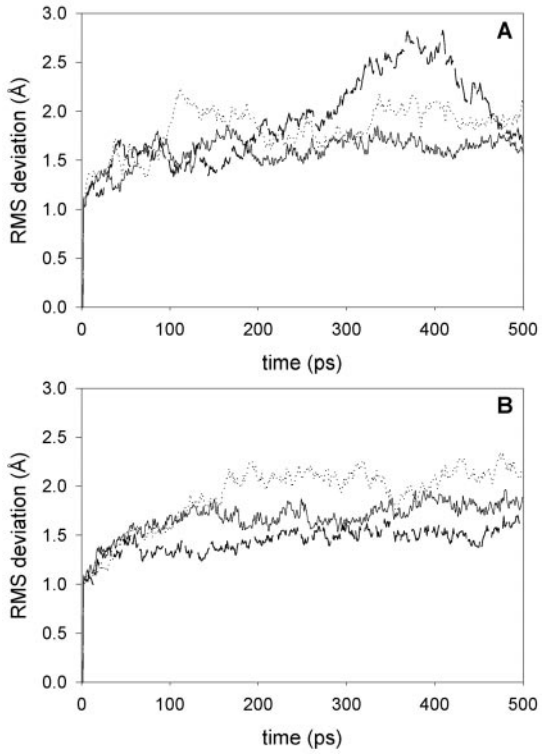

FIG. 1. **r.m.s. deviation of the Cα carbons of the calculated solution GDP-bound (*A*) and GTP-bound (*B*) FtsZ structures from the x-ray determined structure during the molecular dynamics simulations.** *Solid line*, D1 and T1 simulations; *dashed line*, D2 and T2 simulations; *dotted line*, D3 and T3 simulations.

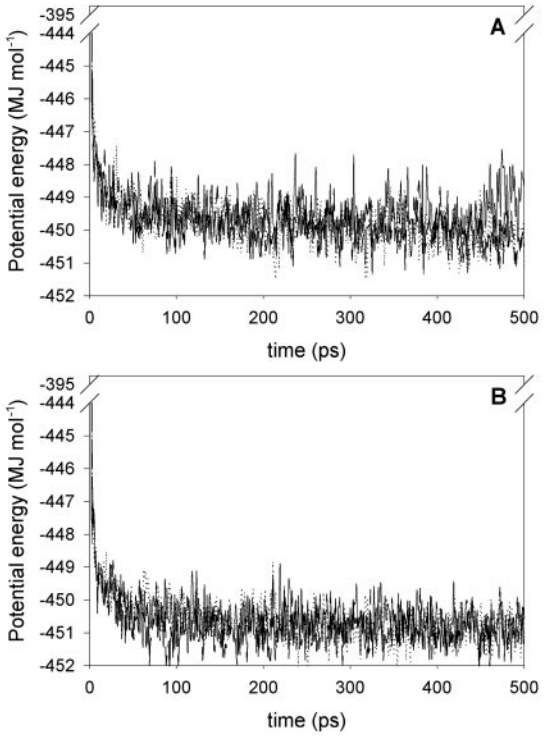

FIG. 2. **Potential energies of GDP-bound (*A*) and GTP-bound (*B*) FtsZ during the molecular dynamics simulations.** *Solid line*, D1 and T1 simulations; *dashed line*, D2 and T2 simulations; *dotted line*, D3 and T3 simulations.

RESULTS

Comparison of the Calculated Solution Structures with the Crystal Structure of FtsZ—Six 500-ps molecular dynamics simulations of *M. jannaschii* FtsZ bound to GDP (D1, D2, and D3 simulations) and GTP (T1, T2, and T3 simulations) were performed to study the conformational effects of the nucleotide bound to the protein (see "Experimental Procedures"). Fig. 3 shows the deviation of the position of the Cα atoms of each

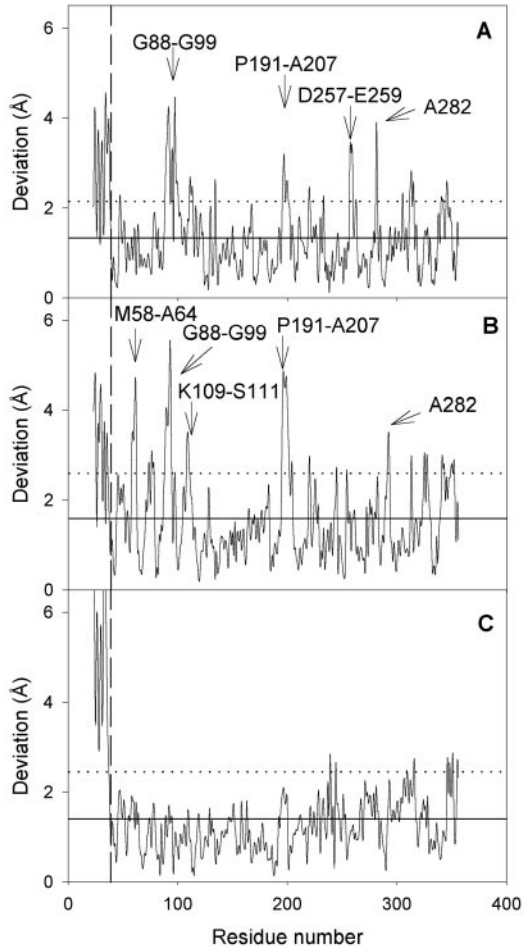

FIG. 3. **Deviation between the positions of the Cα atoms of the averaged calculated solution structures of FtsZ bound to GDP (D1s structure) (*A*) and bound to GTP (T1s structure) (*B*) with respect to the crystal structure; deviation between two GTP-bound calculated structures T1s and T3s (*C*) is shown as comparison.** The *solid lines* represent the r.m.s. deviation of the calculated structures from the x-ray determined structure, the *dotted lines* represent the r.m.s. deviation plus a S.D., and the *vertical dashed lines* mark the H0 helix area, which has a large deviation due to the conformational freedom of Lys^{39}-Ile^{40} bond.

residue of the GDP-bound final average solution structure of the protein after the D1 simulation (D1s structure) and GTP-bound final average solution structure of the protein after the T1 simulation (T1s structure) with respect to the crystallographic structure of FtsZ (Xs). The deviations observed in the other GDP (D2s and D3s) and GTP average structures (T2s and T3s) from the crystal structure are similar to those shown (Fig. 3*C* shows the deviation between two GTP simulations (T1–T3) as a representative control). These changes can be qualitatively described as follows.

First of all, the N-terminal α-helix H0, spanning from Ser^{23} (the first amino acid present in the crystallographic structure) to Lys^{39}, shows large positional differences among all structures (D1s, D2s, D3s, T1s, T2s, T3s, and Xs) due to the rotational freedom of the Lys^{39}-Ile^{40} bond. Nevertheless the structure of the α-helix is completely stable.

The GDP forms show less differences with the crystallographic structure than the GTP forms (as expected since the crystallographic structure is GDP-bound), the observed differences are mainly focused in the area between Gly^{88} and Gly^{99}. Other differences can also be observed in the positions of the loops from Pro^{191} to Ala^{207}, Asp^{257} to Glu^{259}, and at residue Ala^{282} (Fig. 3*A*). Nevertheless differences are smaller than

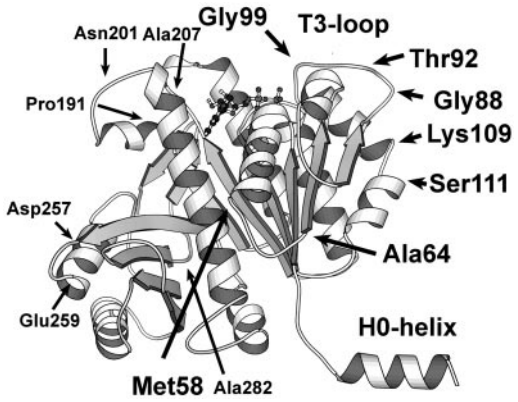

FIG. 4. **Ribbon representation of the x-ray structure of FtsZ on which the relevant structural elements described in the text have been marked (drawing generated with the program MOLSCRIPT; Ref. 58).**

those observed for the GTP-bound forms.

The GTP-bound forms show larger conformational differences with the crystal structure in the zone between Gly^{88} and Gly^{99}, and in the loop from Pro^{191} to Ala^{207}. Additional differences with the crystal structure are located in the zones from Met^{58} to Ala^{64} and Lys^{109} to Ser^{111} (Fig. 3*B*). Fig. 4 shows all these zones labeled onto the crystal structure of FtsZ.

Location of Nucleotide-induced Structural Changes—Since solvent exposed loops may adopt different conformational states, the nine pairs of GDP and GTP structures have been compared to discriminate the more systematic deviations. Fig. 5 shows the deviations between the D1s and T1s, D2s and T2s, and D3s and T3s structures as representative examples. The only differences among D-T pairs that can be systematically observed (at least in six of the nine cases) are reduced to the regions Met^{58}–Ala^{64} (six of nine cases), Gly^{88}–Gly^{99} (nine of nine cases), and Lys^{109}–Ser^{111} (eight of nine cases). Among these, the Gly^{88}–Gly^{99} loop shows considerably larger deviations. The deviations of the Pro^{191}–Ala^{207} loop are not so consistently observed (only four of nine cases).

The GDP and GTP simulated structures have similar flexibilities, except at two points: the segment Gly^{96}–Gly^{99} and Asn^{201}. This fact has been observed in all six simulations. Interestingly, Gly^{99} is one of the more flexible residues in the GDP simulation, becoming more rigid in the GTP simulations. On the other hand, Asn^{201} has increased flexibility in the GTP simulations. As an example, Fig. 6 shows the difference r.m.s. fluctuations of the Cα carbon atoms of the GDP- and GTP-bound structures during the last 200 ps of the D1 and T1 simulations (as the fluctuations of the molecule equilibrate after 150 ps of simulation, the last 200 ps were judged to provide a stable structure).

Fig. 7 shows an insight of the Gly^{88}–Gly^{99} (loop T3) zone of the T1s and D1s structures, the crystal structure of FtsZ, and the electron crystallography structures of α- and β-tubulin. The comparison shows this loop being pulled into a more compact conformation in the presence of the GTP γ-phosphate. A hydrogen bond is formed in the T model between the γ-phosphate of the GTP and the backbone N-H of Gly^{99} of FtsZ (the N-O distances are 2.7 Å in T1s, 3.2 Å in T2s, and 3.1 Å in T3s). The β-phosphate of the GDP is too far away to interact with this NH group (the N-O distances are 4.5 Å D1s, 4.2 Å D2s, 5.5 Å D3s). The loop in the crystal structure (GDP) is, as expected, more close to the GDP model structure than to the GTP model structure.

Modeling Mutations at Loop T3—To prove whether the loop T3 of FtsZ constitutes a switch area, a fluorescent probe may be introduced in the loop, which should have different fluorescent

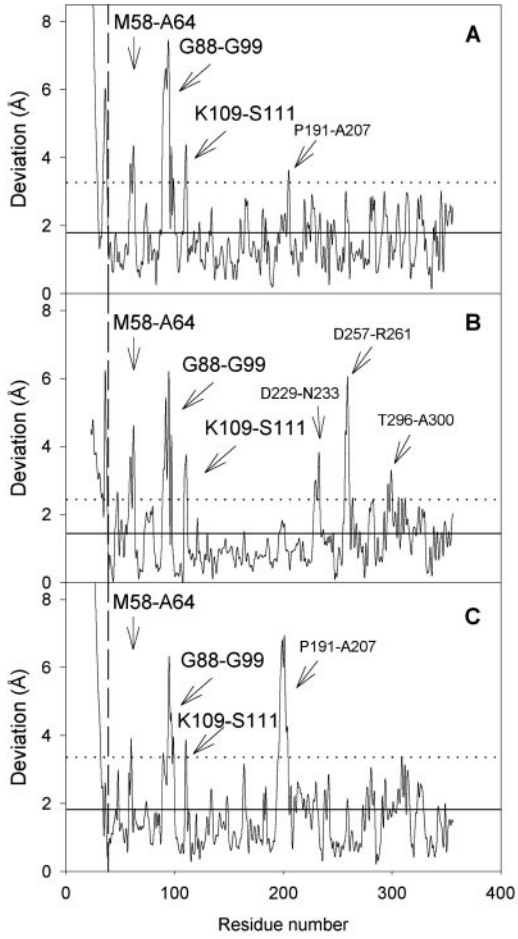

FIG. 5. **Deviation between the positions of the Cα atoms between three different pairs of averaged solution structures of FtsZ bound to GDP and GTP.** Figure shows deviation between structures D1s and T1s (*A*), deviation between structures D2s and T2s (*B*), and deviation between D3s and T3s structures (*C*). The *solid lines* represent the r.m.s. deviation between the calculated GDP-bound and GTP-bound structures, the *dotted lines* represent the r.m.s. deviation plus a S.D., and the *dashed lines* mark the H0 helix area, which has a large deviation due to the conformational freedom of Lys^{39}-Ile^{40} bond.

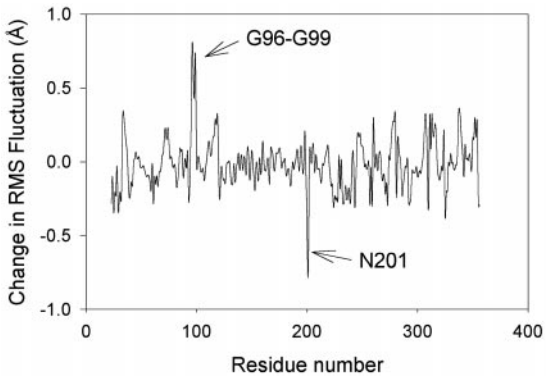

FIG. 6. **Difference in the r.m.s. fluctuations of the Cα atoms of the calculated FtsZ GDP- and GTP-bound forms during the last 200 ps of the D1 and T1 simulations.** Positive values indicate increased flexibility in the D1 simulation, negative values increased flexibility in the T1 simulation.

properties in the GDP- and GTP-bound states. This was the case, for example, in the Y32W mutant of Ha-Ras-p21 (22) employed to monitor the activation state of that protein. Such a mutant with a fluorescent residue in the putative effector loop would be of great interest for studying the activation

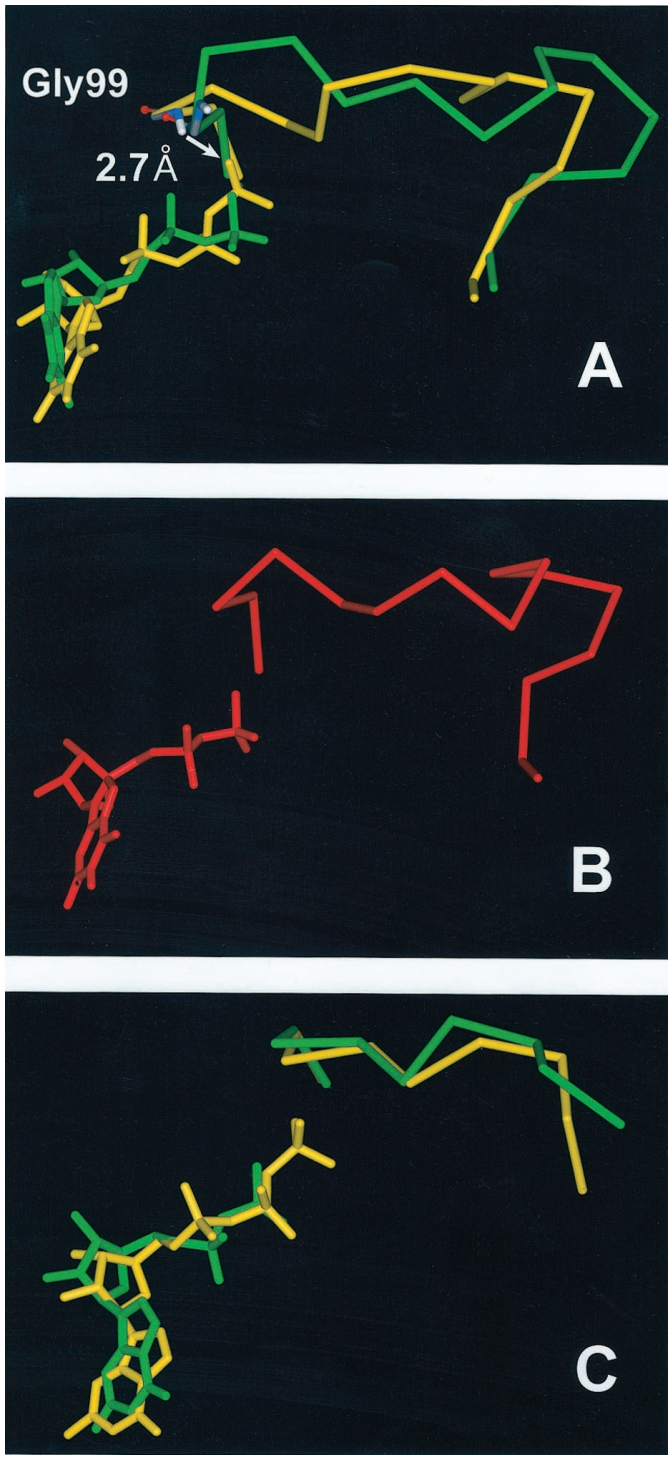

FIG. 7. **Detail of the conformation of loop T3.** Superposition of loop T3 of the FtsZ GTP-bound T1s structure (*yellow*), with the one of the GDP-bound D1s structure (*green*) (*A*), loop T3 in the x-ray structure of FtsZ (*red*) (*B*), superposition of loop T3 of the α-tubulin monomer (GTP-bound, *yellow*), with the one of the β-tubulin monomer (GDP-bound, *green*) (*C*).

mechanisms of the FtsZ structural GTPase since the active and inactive states could be detected with a simple spectrofluorometric test.

The loop T3 is very rich in small residues: 5 glycines and 1 alanine. Since these residues have special allowed areas in the Ramachandran plot, substitution of them by a large group would cause structural perturbations. The loop is also rich in basic residues, 2 lysines and 1 arginine in 11 residues. Since mutating a charged residue in a presumably active area may

TABLE I
Average molecular mass of M. jannaschii FtsZ (sedimentation equilibrium)

Protein and buffer	Mw,a_a		
	2 μM FtsZ	5 μM FtsZ	10 μM FtsZ
WT (Buffer A, 50 mM KCl)[b]	80,000 ± 3000	92,000 ± 1000	95,000 ± 2000
T92W-W319Y (Buffer A, 50 mM KCl)	65,000 ± 3000	80,000 ± 2000	88,000 ± 2000
WT (Buffer A, 500 mM KCl)	47,000 ± 1000	58,000 ± 1000	66,000 ± 1000
T92W-W319Y (Buffer A, 500 mM KCl)	48,000 ± 2000	58,000 ± 1000	62,000 ± 2000

[a] Mw,a, whole cell apparent average molecular weight of the species in solution.
[b] Buffer A: 50 mM Tris, 50 μM EDTA, 10 μM GDP, pH 8.0.

result in loss of activity, only three candidate residues were left: Leu^{91}, Thr^{92}, and Leu^{95}. These three residues showed large differences (3–4 Å) in position between the crystal structure and both *in silico* solution structures (Fig. 3), and even larger (about 6 Å) between the GDP- and GTP-calculated structures (Fig. 5). The mutation of these residues into the natural fluorophore, tryptophan, was modeled into the final structures of the GDP and GTP simulations using the WHATIF software package (44). In the resulting mutated model structures the same large conformational differences in the position of the tryptophans were observed. The larger differences (which may imply larger differences in fluorescent properties) correspond to Trp^{92}, which is more exposed to the solvent in the GTP-bound form than in the GDP-bound models. In addition, this residue is sufficiently far away from the γ-phosphate (11.5 ± 2.1 Å in the GTP conformations) and β-phosphate (18.5 ± 3.1 Å in the GDP conformations), so that potential changes in its fluorescent properties can be assigned to conformational changes in the tryptophan environment. *M. jannaschii* FtsZ contains one tryptophan at position 319, which must be removed to have a single tryptophan mutant whose spectral changes are easier to interpret. The double mutant T92W-W319Y was constructed, expressed, and purified as described under "Experimental Procedures."

Wild Type and T92W-W319Y FtsZ from M. jannaschii Have Similar Nucleotide Binding Capacity, Association State, and Secondary Structure—The wild type protein (purified by breaking the cells by sonication) contained 0.70 mol of nucleotide/mol of FtsZ, of which 19.5% was GTP and 80.5% GDP. When purified by heat shock (15), it had a similar nucleotide composition (0.80 nucleotide per FtsZ, 21.5% GTP and 78.5% GDP). The T92W-W319Y FtsZ mutant contained less nucleotide (0.28 nucleotide per FtsZ, 39.6% GTP and 60.5% GDP). However, both proteins retained full nucleotide binding activity. The nucleotide content increased both in the wild type and T92W-W319Y FtsZ up to 1.01 per FtsZ (3% GTP, 97% GDP in both cases) after 1 h of incubation at 4 °C with 1 mM GDP and further equilibration in buffer A plus 500 mM KCl.

The relative affinity of these proteins for GDP and GTP was checked as described (see "Experimental Procedures"). Both the wild type and the mutant exchange GDP for GTP with a similar affinity ratio of 4.25:1 ($K_{GTP\text{-}FtsZ}$:$K_{GDP\text{-}FtsZ}$) (the total nucleotide content remained 1.01 per FtsZ). This affinity ratio is modified by 1 mM $MgCl_2$, to 1.45:1 ($K_{GTP\text{-}FtsZ}$:$K_{GDP\text{-}FtsZ}$).

Since it is known that tubulin binds divalent cations (45–47), *M. jannaschii* FtsZ requires divalent cations to form filaments (48) and FtsZ from *E. coli* requires Mg^{+2} to hydrolyze GTP but not to assemble into filaments (49) the content of Mg^{+2} and Ca^{+2} of the wild type protein (both purification procedures) and of the double mutant were measured. No Mg^{+2} or Ca^{+2} was found. This was expected since the last step of purification is a gel filtration in a buffer containing 1 mM EDTA, and coincides with the crystallographic structure of FtsZ in which no metallic cations were observed. The residual total Mg^{+2} and Ca^{+2} was found to be lower than 1 and 5 μM, respectively, which implies free concentrations below 13.8 and 1.3 nM, respectively, in the 50 μM EDTA containing experimental buffer employed.

The oligomerization state of the wild type and mutant protein was studied using analytical ultracentrifugation. The apparent weight average molecular weight was measured by sedimentation equilibrium at different ionic strength and protein concentrations (Table I). At high ionic strength, 500 mM KCl, both proteins are close to monomeric state if the protein concentration is kept low enough. At low ionic strength, the mutant has a lower self-association. To check if the nucleotide bound to the protein may affect its aggregation state, sedimentation velocity experiments were done. The measured sedimentation coefficients of WT and mutant proteins in buffer A, 500 mM KCl, are not affected by the nucleotide bound to them (Table II). The values at 2 μM FtsZ correspond to globular particles with a relative frictional coefficient ratio of 1.2 ± 0.1.

To check whether the double mutation introduces a change in the secondary structure of the protein, circular dichroism (CD) spectroscopy was performed. Both spectra from *M. jannaschii* wild type and the double mutant FtsZ were identical (data not shown), indicating that no major change in secondary structure is caused by these mutations. These spectra (data not shown) are typical for αβ-proteins and are actually similar to those measured for *E. coli* FtsZ (33) and tubulin (6). The secondary structure content estimated using the convex constraint algorithm method (32 ± 4% α-helix, 19 ± 9% β-sheet, 45 ± 8% other) is almost identical to that of tubulin (6).

Nucleotide-induced Changes in the Tryptophan Fluorescence of T92W-W319Y FtsZ Monomers—The single tryptophan residue (Trp^{319}) of *M. jannaschii* FtsZ is far away from the nucleotide binding area. Fig. 8 shows the tryptophan fluorescence emission spectra of the wild type and T92W-W319Y mutant of FtsZ (2 μM monomers) in their GDP- and GTP-bound states. Trp^{319} has a much larger quantum yield than Trp^{92} (3–4 times more fluorescence intensity), but its fluorescence is not modified by the nucleotide bound.

As predicted, the tryptophan introduced at position 92 is very sensitive to the nucleotide bound. The tryptophan in the GTP state has 30% more fluorescence intensity than with GDP and its emission maximum at 348 nm, while in the GDP state the maximum is at 343 nm (Fig. 8*B*). The change in intensity is linearly dependent on the nucleotide content of the protein (Fig. 8*C*). Since the change in the emission maximum is not too large, this indicates that the difference in intensity is due to the different quantum yields of the GDP and GTP states of the FtsZ monomers. The same intensity change was measured at higher FtsZ concentrations (20 μM). Addition of up to 5 mM $MgCl_2$ to the solutions of Fig. 8 produces no appreciable change in the fluorescence of the tryptophan neither in the GDP-bound nor in the GTP-bound states, indicating that the binding of the divalent cation (which affects GTP/GDP affinity ratio) does not influence the conformation of loop T3.

The fluorescence emission maximum of Trp^{92} shows a large shift to the red compared with Trp^{319} and typical values in native proteins (50), indicating a large accessibility of the residue to the solvent (in the GTP-bound state, this residue has an emission maximum coincident with that of tryptophan in wa-

TABLE II
Sedimentation coefficients of M. jannaschii FtsZ (sedimentation velocity)

Protein and buffer	$S_{20,w}$			
	2 μM FtsZ		10 μM FtsZ	
	GDP[a]	GTP[b]	GDP[a]	GTP[b]
WT (Buffer A, 50 mM KCl)	4.6 ± 0.1	4.5 ± 0.1	5.5 ± 0.1	5.5 ± 0.1
T92W-W319Y (Buffer A, 50 mM KCl)	4.2 ± 0.1	4.0 ± 0.1	5.6 ± 0.1	5.6 ± 0.1
WT (Buffer A, 500 mM KCl)	3.3 ± 0.1	3.2 ± 0.1	3.8 ± 0.1	3.8 ± 0.1
T92W-W319Y (Buffer A, 500 mM KCl)	3.3 ± 0.1	3.2 ± 0.1	3.8 ± 0.1	3.6 ± 0.1

[a] 20 μM GDP was added to the sample just before the run.
[b] 20 μM GTP was added to the sample just before the run.

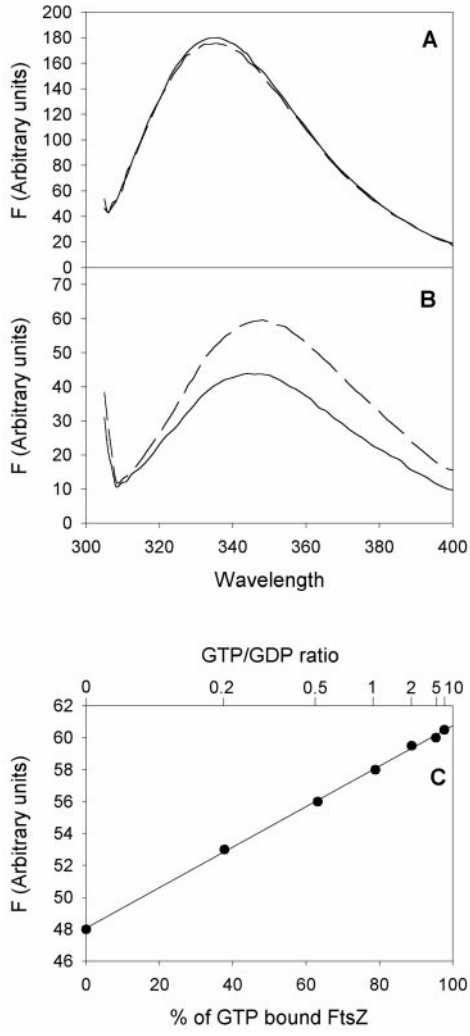

FIG. 8. *A* and *B*, fluorescence emission spectra (λ_{exc} = 295 nm) of 2 μM WT-FtsZ (*A*) from *M. jannaschii* in buffer A 500 mM KCl, plus 50 μM GDP (*solid line*), or plus 50 μM GTP (*dashed line*) and 2 μM T92W-W319Y-FtsZ (*B*) in buffer A 500 mM KCl, plus 50 μM GDP (*solid line*) or plus 50 μM GTP (*dashed line*). *C*, fluorescence intensity λexc = 295 nm, λems = 348 nm) of 2 μM T92W-W319Y-FtsZ in buffer A (500 mM KCl, plus 50 μM guanine nucleotide). GDP and GTP mixed in different proportions shown in the *upper x axis*). The percentage of GTP in the total nucleotide content of FtsZ is represented in the *lower x axis*).

ter). The mean solvent accessibility of the side chain of Trp^{92}, modeled into the GTP simulated structures, is 25.3 ± 1.2 Å^2, and 18.1 ± 1.1 Å^2 when modeled into the GDP structures. The mean accessibility of the Trp^{319} side chain of the wild type protein is lower, 15.8 ± 0.6 Å^2. The positions of the different maxima of the emission spectra (348 nm for T92W-W319Y GTP-bound, 343 nm for T92W-W319Y GDP-bound, 335 nm for wild type) are qualitatively concordant with these solvent accessibilities.

DISCUSSION

Conformational Differences between the Solution Structures of GDP and GTP-bound FtsZ Calculated from Its Crystal Structure with Molecular Dynamics—The main goal of this work was to investigate how the presence or absence of the γ-phosphate of the nucleotide bound to its site on FtsZ affects the protein conformation. To do this, six 500-ps free molecular dynamics simulations were performed, with either GDP or GTP bound at the nucleotide site, employing the coordinates of the x-ray determined structure of the GDP-bound protein.

The simulated structures equilibrate relatively rapidly (in around 200 ps) and deviate very little from the x-ray structure, indicating the quality of the simulation. The GDP-bound form shows a slightly lower r.m.s. deviation from the x-ray determined structure than the GTP one as expected. The energy of the calculated structures decreases quite rapidly, indicating the quality of the refinement of the x-ray structure. The GTP-bound calculated structures show lower energies, which suggest increased stability of this form.

The calculated structures consistently deviate from the x-ray structure in the loop from Gly^{88} to Gly^{99}. This zone deviates up to 4 Å for some residues in the GDP-bound calculated structures and up to 6 Å in the GTP-bound ones. This loop is quite well defined in the crystallographic structure and shows the lowest *B*-factors of the molecule, so that the large differences calculated should indicate an influence of the nucleotide in the conformation of the loop.

The structure of the loop in the calculated solvated GDP form is slightly different from the crystal structure. The nucleotide bound to the purified protein is mainly GDP (80%); nevertheless, a significant percentage of the protein (20%) has GTP bound, which explains why a weak electron density of the γ-phosphate could be observed in fresh crystals (14). In the crystal structure, loop T3 is packed with contacts with other two molecules; contacts include the areas from Leu^{29} to Ala^{38} in the H0 helix and other residues in the vicinity of this helix (Asp^{121}, Asp^{123}, Lys^{148}, Leu^{153}, Asp^{235}, Lys^{240}) of one molecule, and a part of the loop T3 and the nucleotide binding cup Gly^{166}–Arg^{169} of other molecule. It might be possible that this loop is fixed in one of its possible conformations by these crystal restraints, since neither heterogeneity and nor large conformational changes between fresh and old crystals were observed (14). Nevertheless, it must be pointed out that the conformation of the loop in the GDP-bound state is more close to the crystallographic than the GTP-bound one, and the conformation of the loop in the solvated calculated structures is very trustable since three independent simulations gave the same result.

The molecular dynamics results strongly suggest that the structure of the zone between Gly^{88} and Gly^{99} depends on the presence of the nucleotide γ-phosphate. Several residues in this loop deviate about 6 Å between the calculated GDP and GTP structures. This deviation is probably due to the hydrogen bond that is formed between the γ-phosphate of GTP bound and the

N-H group of residue Gly[99] (Fig. 7*A*), which fixes this residue therefore decreasing its flexibility (Fig. 6). This pulls on the T3 loop and stabilizes a more closed conformation similar to the one observed in the tubulin monomers which are fixed in the active state. The β-phosphate of the GDP is too far away to form this H-bond (Fig. 7, *A* and *B*). Although there is not an exact equivalent of loop T3 in Ha-*ras*-p21, its position in the FtsZ molecule is equivalent to that occupied by the switch II region of this GTPase (which has a fold partially resembling the GTP-binding domain of FtsZ and tubulin although its topology is different).

Loop T3 is apparently able to transmit the signal of the presence of the γ-phosphate to a small area Lys[109]–Ser[111], which forms a hinge between the two segments of helix H3 (structurally equivalent to helix α2 of Ha-*ras*-p21). Both segments of the helix form a 110° angle in the crystal FtsZ structure, while in the electron crystallography tubulin structure they form an approximate angle of 150° (both monomers). In the GTP-bound modeled structures T1s, T2s, and T3s, this hinge opens and the helical segments form an angle of 125 ± 5°, while in the GDP-bound simulations the hinge closes to render a 100 ± 5° angle between both segments. Changes in length and orientation in the structurally equivalent (although much shorter) α2 helix of Ha-*ras*-p21 upon GTP binding can be observed between both crystal structures (the helix is longer and is more closely packed with the β-sheet in the GTP-bound structure) (51, 52). This may suggest a related intramolecular signal transmission mechanism. There is a distant FtsZ zone, from Met[58] to Ala[64], that also seems to be sensitive to the presence of the γ-phosphate of the nucleotide. Note that other zones (including possible domain movement), which have not been detected by the molecular dynamics analysis, may change as well in response to the presence of the γ-phosphate.

Loop T3 as Switch Element of FtsZ and Tubulin—To confirm the molecular dynamics predictions, a mutant in which a fluorescent probe is introduced at loop T3 of FtsZ was constructed. The single tryptophan of the protein at position 319 has been replaced by a tyrosine, and a new tryptophan has been introduced at position 92. The mutant behaves as predicted, showing appreciable changes in fluorescent intensity and in the position of the tryptophan emission maximum depending on the bound nucleotide. Since from the relevant tryptophan quenchers that can be found in proteins (disulfide bridges, protonated histidine, cysteine, tyrosine, and carbonyl carbons; Ref. 53) only the carbonyl carbons of the peptide bonds are present in the environment of Trp[92], the change in fluorescence intensity should really indicate a conformational change of the main chain of the loop. The 5-nm blue shift of the emission maximum is interpreted as an increase in exposure to the solvent of the Trp side chain, as observed in the molecular dynamics model structures (see "Results").

Loop T3 is highly homologous between FtsZ and tubulin, although the first part of the loop is seven residues longer in FtsZ (16). Since the x-ray structure of a GTP-bound form of FtsZ is not presently available, it is not possible to compare the structure of loop T3 in the GTP- and GDP-bound states of FtsZ. Nevertheless, the GTP-bound and GDP-bound calculated structures can be compared with the GDP-bound FtsZ x-ray structure and with the α- and β-tubulin structures (15). The latter should correspond to an active state, since α-tubulin is bound to GTP and β-tubulin is fixed in a Zn^{2+}-induced polymer grown from GTP-bound tubulin and stabilized with taxol.

The comparison of the GDP and GTP calculated average structures (Fig. 7*A*) and the crystal structure of FtsZ (Fig. 7*B*) shows that the position of the loop T3 in the GDP-bound form is even more displaced toward the outer part of the protein than in the crystal structure, whereas the structure of the GTP-bound form is more displaced toward the nucleotide in central part of the interface. This points out that the forces produced by the presence of the γ-phosphate should change the conformation of the loop toward this position in the active form of the protein, which is fully supported by the fluorescence results with the T92W FtsZ mutant.

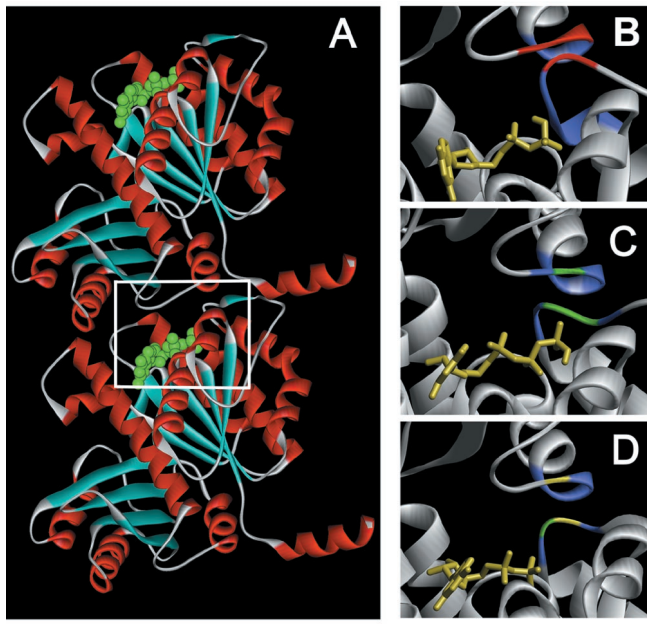

FIG. 9. *A*, model of FtsZ association constructed as described by Löwe and Amos (48), using the crystal structure 1FSZ as monomer. *B*, detail of the area of collision between loop T3, helix H8, and loop T7 in a model of FtsZ association constructed in the same way using the GDP-bound averaged calculated D1s structure as monomer. *C* and *D*, detail of the same area in the model constructed using the GTP-bound averaged calculated T1s structure as monomer (*C*), and using the crystal structure 1FSZ as monomer (*D*). Note that the area of collision around the nucleotide binding is represented in a slightly different perspective for better visualization purposes. The residues are represented in colors indicating the degree of the collision. *Gray* means no collision, *blue* means structural collision between the side chain of the residues, *green* means minor structural collision between the backbones (distance between the atoms larger than 1 Å less than the sum of Van der Waals radii), *yellow* means large structural collision between the backbones (distance between the atoms between 1 and 2 Å less than the sum of Van der Waals radii), and *red* means superposition of the backbones (distance between the smaller than 2 Å less than the sum of Van der Waals radii).

FtsZ monomers have been modeled into an electron microscopy density map of FtsZ filaments (48), using as a starter model the structure of the tubulin dimer (15). In this manner monomer features may be applied to the polymer. Fig. 9 shows a model of FtsZ-FtsZ contact constructed as described (48), using the crystal structure of 1FSZ. The view is equivalent to a microtubule protofilament seen from outside the microtubule. As can be seen, loop T3 is located at one side of the putative contact interface between two FtsZ molecules. Loop T3 has contacts with the beginning of helix H8 and a collision with the end of loop T7 of the contacting FtsZ molecule as described (48). Additional contacts can be observed with helix H0, but as seen in this work the helix has a relatively large conformational freedom, and it is probably in a different position in the filament, as pointed out by the fact that helix H0 density does not fit in the electron microscopy map and must be moved to fill the empty part of the density, which lies nearby (48).

Fig. 9 (*B–D*) shows a detail of the loop T3-helix H8 contact area in the same model of FtsZ-FtsZ association (Fig. 9*A*) built with the GDP, GTP, and crystal structures. The contact area in

T1s (Fig. 9*C*) is very similar to the one of the crystal structure model (Fig. 9*D*) (minor collisions with helix H8 and loop T7 are observed). However, the conformation of loop T3 in the D1s structure (Fig. 9*B*) should push helix H8 upward, thus bending the filament; otherwise, large superpositions of both main chains (represented by the *red* coloring) arise. It is thus conceivable that loop T3 conformation, which can switch between the characteristic GTP and GDP states, may modulate the bending of the FtsZ filament, inhibiting assembly. Note that these representations are just models since an accurate simulation of the effect of the conformational changes in the interface would require accurate structures of the contact surface, which are not available. In any case, there is evidence that GTP favors the straight FtsZ filament conformation and GDP the curved conformation, so that GTP hydrolysis might be used to generate force for the constriction of the FtsZ ring during cell division (54).

A comparison between the structure of loop T3 in FtsZ, α- and β-tubulin (Fig. 7) shows different conformations of the loop. In the GDP-bound FtsZ in inactive conformation, loop T3 is displaced toward the outer part of the nucleotide binding domain, while the conformation of the loop in the active conformation of tubulin is displaced toward the inner part of the molecule and it is more compact. Nevertheless, this comparison has to be taken with care due to the gap present in the tubulin sequences. Loop T3 of tubulin may participate both in the longitudinal contact interface between tubulin dimers in the protofilament as well as in the contact between adjacent protofilaments in the microtubule (16, 55). Therefore, its conformation may easily control the assembly of the tubulin molecule. If the position of loop T3 in GDP-tubulin were similar to the one predicted by the simulation for FtsZ, it might bend the protofilament in a direction perpendicular to its axis. Structures resulting from bending of protofilaments have been actually observed in the small angle x-ray scattering structure of tubulin double rings assembled from GDP-tubulin (56) and in the 4-Å crystal structure of the complex of two GDP-tubulin dimers with a stathmin-like domain (57), and proposed to reflect the structural change between the active (straight) and inactive (curved) conformations of tubulin. Nevertheless, it must be pointed out that the bending direction observed is different in both cases. In GDP-induced tubulin double rings, this bending appears tangent to the microtubule surface, as is predicted to be induced by the movement of loop T3, whereas, in the stathmin complex, the tubulin curvature appears in an oblique with respect to the microtubule surface.

Acknowledgments—We thank Dr. Jan Löwe for kindly providing the plasmid containing FtsZ from *M. jannaschii*, Dr. German Rivas (Centro de Investigaciones Biológicas (CIB)) for support and useful discussions Dr. Alicia Prieto (CIB) for the mass spectroscopy, Dr. Carlos Alfonso (CIB) and S. Zorrilla for analytical ultracentrifugation experiments, Pilar Palacios (Centro Nacional de Biotecnología) for technical assistance, and the CIB biocomputing service for computing time.

REFERENCES

1. Lee, J. C., and Timasheff, S. N. (1975) *Biochemistry* **14,** 5183–5187
2. Bi, E., and Lutkenhaus, J. (1991) *Nature* **354,** 161–164
3. De Boer, P., Crossley, R., and Rothfield, L. (1992) *Nature* **359,** 254–256
4. RayChaudhuri, D., and Park, J. T. (1992) *Nature* **359,** 251–254
5. Sage, C. R., Dougherty, C. A., Davis, A. S., Burns, R. G., Wilson, L., and Farrel, K. W. (1995) *Biochemistry* **34,** 7409–7419
6. De Pereda, J. M., Leynadier, D., Evangelio, J. A., Chacón, P., and Andreu, J. M. (1996) *Biochemistry* **35,** 14203–14215
7. Amos, L., and Klug, A. (1974) *J. Cell Sci.* **14,** 523–549
8. Mukherjee, A., and Lutkenhaus, J. (1994) *J. Bacteriol.* **176,** 2754–2758
9. Erickson, H. P., Taylor, D. W., Taylor, K. A., and Bramhill, D. (1996) *Proc. Natl. Acad. Sci. U. S. A.* **93,** 519–523
10. McNiven, M. A., Cao, I., Pitts, K. R., and Yoon, I. (2000) *Trends Biochem. Sci.* **25,** 115–120
11. Erickson, H. P. (2000) *J. Cell Biol.* **148,** 1103–1105
12. Margolin, W. (2000) *Curr. Biol.* **10,** 328–330
13. Hinshaw, J. E., and Schmid, S. L. (1995) *Nature* **374,** 190–192
14. Löwe, J., and Amos, L. A. (1998) *Nature* **391,** 203–206
15. Nogales, E., Wolf, S. G., and Downing, K. (1998) *Nature* **391,** 199–203
16. Nogales, E., Downing, K. H., Amos, L., and Löwe, J. (1998) *Nat. Struct. Biol.* **5,** 451–458
17. Adari, H., Lowy, D. R., Willumsen, B. M., Der, C. J., and McCormick, F. (1988) *Science* **240,** 518–521
18. Scheffzek, K., Reza-Ahmadian, M., and Wittinghoffer, A. (1998) *Trends Biochem. Sci.* **23,** 257–262
19. Schlitter, J., Engels, M., Krüger, P., Jacoby, E., and Wolmer, A. (1993) *Mol. Sim.* **10,** 291–309
20. Díaz, J. F., Wroblowski, B., and Engelborghs, Y. (1995) *Biochemistry* **34,** 12038–12047
21. Díaz, J. F., Wroblowski, B., Schlitter, J., and Engelborghs, Y. (1997) *Proteins Struct. Funct. Genet.* **28,** 434–451
22. Díaz, J. F., Sillen, A., and Engelborghs, Y. (1997) *J. Biol. Chem.* **272,** 23138–23143
23. Kuppens, S., Díaz, J. F., and Engelborghs, Y. (1999) *Protein Sci.* **8,** 1860–1866
24. Díaz, J. F., Escalona, M. M., Kuppens, S., and Engelborghs, Y. (2000) *Protein Sci.* **9**, 361–368
25. Madigan, M. T., Martinko, J. M., and Parker, J. (1997) *Brock Biology of the Microorganisms*, pp. 741–768, Prentice Hall, Inc., Hertfordshire, U. K.
26. Fusi, P., Goosens, K., Consonni, R., Grisa, M., Puricelli, P., Vecchio, G., Vanoni, M., Zetta, Z., Heremans, K., and Tortora, P. (1997) *Proteins Struct. Funct. Genet*. **25,** 381–390
27. Weiner, M. P., Costa, G. L., Schoettlin, W., Cline, J., Mathur, E., and Bauer, J. C. (1994) *Gene* (*Amst.*) **151,** 119–123
28. Löwe, J. (1998) *J. Struct. Biol.* **124,** 235–243
29. Laemmli, U. K. (1970) *Nature* **227,** 680–685
30. Díaz, J. F., and Andreu, J. M. (1993) *Biochemistry* **22,** 2747–2755
31. Pace, C. N., and Schmid, F. X. (1997) in *Protein Structure: A Practical Approach* (Creighton, T., ed) 2nd Ed., pp. 253–259, Oxford University Press, Oxford
32. Perczel, A., Park, K., and Fasman, G. D. (1992) *Anal. Biochem.* **203,** 83–93
33. Rivas, G., López, A., Mingorance, J., Ferrándiz, M. J., Zorrilla, S., Minton, A. P., Vicente, M., and Andreu, J. M. (2000) *J. Biol. Chem.* **275,** 11740–11749
34. Minton, A. (1994) in *Modern Analytical Ultracentrifugation* (Schuster, T., and Laue, T., eds) pp. 81–93, Birkhauser Boston, Inc., Cambridge, MA
35. Philo, J. S. (1997) *Biophys. J.* **72,** 435–444
36. Berman, H. M., Westbrook, J., Feng, Z., Gilliland, G., Bhath, T. N., Weissig, H., Shindyalov, I. N., and Bourne, P. E. (2000) *Nucleic Acids Res.* **28,** 235–242
37. Van Gunsteren, W. F., Billeter, S. R., Eising, A. A., Hünenberger, P. H., Krüger, P., Mark, A. E., Scott, W. R. P., and Tironi, I. G. (1997) *Biomolecular Simulation: The GROMOS 96 Manual and User Guide*, BIOMOS b.v., Zürich
38. Berendsen, H. J. C., Postma, J. P. M., Van Gunsteren, W. F., and Hermans, J. (1981) *Interaction Models for Water in Relation to Protein Hydration Intramolecular Forces* (Pullman, B., ed) pp. 331–342, Reidel, Dordrecht, The Netherlands
39. Levitt, M., and Lifson, S. (1969) *J. Mol. Biol.* **46,** 269–279
40. Berendsen, H. J. C., Postma, J. P. M., Van Gunsteren, W. F., Dinola, A., and Haak, J. R. (1984) *J. Chem. Phys.* **81,** 3684–3690
41. Ryckaert, J. P., Ciccotti, G., and Berendsen, H. J. C. (1977) *J. Comput. Phys.* **23,** 327–341
42. Van Gunsteren, W. F., and Berendsen, H. J. C. (1977) *Mol. Phys.* **34,** 1311–1327
43. Krüger, P., Lüke, M., and Szameit, A. (1991) *Comput. Phys. Commun.* **62,** 371–380
44. Vriend, G. (1990) *J. Mol. Graphics* **8,** 52–56
45. Lee, J. C., and Timasheff, S. N. (1977) *Biochemistry* **16,** 1754–1764
46. Correia, J. J., Baty, L. T., and Williams, R. C., Jr. (1987) *J. Biol. Chem.* **262,** 17278–17284
47. Menéndez, M., Rivas, G., Díaz, J. F., and Andreu, J. M. (1998) *J. Biol. Chem.* **273,** 167–176
48. Löwe, J., and Amos, L. A. (1999) *EMBO J.* **18,** 2364–2371
49. Mukherjee, A., and Lutkenhaus, J. (1999) *J. Bacteriol.* **181,** 823–832
50. Lakowicz, J. R. (1984) *Principles of Fluorescence Spectroscopy*, pp. 341–381, Plenum Press, New York
51. Tong, L. A., de Vos, A. M., Milburn, M. V., and Kim, S. H. (1991) *J. Mol. Biol.* **217,** 503–516
52. Pai, E. F., Krengel, U., Petsko, G. A., Goody, R. S., Kabsh, W., and Wittinghoffer, A. (1990) *EMBO J.* **9,** 2351–2359
53. Sillen, A., Díaz, J. F., and Engelborghs, Y. (2000) *Protein Sci.* **9,** 158–169
54. Lu, C., Reedy, M., and Erickson, H. P. (2000) *J. Bacteriol.* **182,** 164–170
55. Nogales, E., Whittaker, M., Milligan, R. A., and Downing, K. H. (1999) *Cell* **96,** 79–88
56. Díaz, J. F., Pantos, E., Bordas, E., and Andreu, J. M. (1994) *J. Mol. Biol.* **238,** 214–225
57. Gigant, B., Curmi, P. A., Martin-Barbey, C., Charbaut, E., Lachkar, S., Lebeau, L., Siavoshian, S., Sobel, A., and Knossow, M. (2000) *Cell* **102,** 809–816
58. Kraulis, P. J. (1991) *J. Appl. Crystallogr.* **24,** 946–950